Morphological effects on dielectric properties of poly(vinylidene fluoride-*co*-hexafluoropropylene) blends and multilayer films

Jung-Kai Tseng, Kezhen Yin, Zhongbo Zhang, Matthew Mackey, Eric Baer, and Lei Zhu*

Department of Macromolecular Science and Engineering, Case Western Reserve University, Cleveland, Ohio 44106-7202, United States

Email address: lxz121@case.edu (L. Zhu).

Abstract: Compared with chemical modification of ferroelectric poly(vinylidene fluoride) (PVDF) for electric energy storage, polymer blends, whether miscible or immiscible, represent a much easier approach to suppress the ferroelectricity of PVDF. In this study, we explored both miscible [i.e., poly(methyl methacrylate) or PMMA] and immiscible (i.e., polycarbonate or PC) blends with poly(VDF-*co*-hexafluoroethylene) [P(VDF-HFP)], as well as the PC/P(VDF-HFP) multilayer films. For miscible PMMA/P(VDF-HFP) blend films, the addition of PMMA significantly decreased the crystallinity of P(VDF-HFP). At a high PMMA content of ca. 40 wt.%, the stretched PMMA/P(VDF-HFP) blend films started to exhibit the linear dielectric behavior with suppressed ferroelectricity. For the immiscible PC/P(VDF-HFP) blend films, a high PC content of ~50 vol.% was required to suppress the ferroelectricity in P(VDF-HFP). Instead, the PC/P(VDF-HFP) multilayer films started to show linear hysteresis loops when the content of P(VDF-HFP) was only 30 vol.%. More importantly, the PC/P(VDF-HFP) multilayer films exhibited significantly higher breakdown strength than the blend films. This could be attributed to the perpendicular interfaces (with respect to the applied electric field), which serve as effective blocks for hot electrons injected from the metal electrodes to pass through the film. From this study, compared to conventional miscible and immiscible blends, multilayer films are promising for next generation film capacitors, aiming to achieve high temperature tolerance, high energy density, and low loss simultaneously.

Keywords: poly(vinylidene fluoride-*co*-hexafluoropropylene), polymer blends, multilayer films

1. Introduction

High performance polymer dielectric films are highly desirable for advanced electronic and power applications such as DC link capacitors in fully or hybrid electric vehicles.[1-3] Current state-of-the-art polymer film is the biaxially oriented polypropylene (BOPP) film, primarily owing to its extremely low dielectric loss (e.g., dissipation factor tanδ ~ 0.0002), high breakdown strength (730 MV/m at a 2 cm^2 test area), and long lifetime.[4-6] However, the temperature rating for BOPP films is limited at 85 °C, above which its lifetime significantly decreases without derating the operating voltage.[7] In addition, the energy density of BOPP is relatively low because of its low dielectric constant of only 2.25. To address these issues, tremendous research efforts have been dedicated to develop new high temperature, high dielectric constant, and low loss polymer dielectrics for electric energy storage applications.[8-12]

Poly(vinylidene fluoride) (PVDF) and its random copolymers have high dielectric constant in the range of 10-12.[13-15] Although biaxially oriented PVDF films have been commercially developed (as thin as 3-4 μm), they cannot be used for film capacitors simply because of significant ferroelectricity in PVDF crystals.[9, 16-17] To suppress ferroelectricity for electric energy storage, modification of PVDF and its random copolymers has been carried out. The first strategy is to terpolymerize a large termonomer such as 1,1-chlorofloroethylene (CFE) or chlorotrifluoroethylene (CTFE) with vinylidene fluoride (VDF) and trifluoroethylene (TrFE).[9-10, 18-20] Because of the inclusion of the large termonomers inside P(VDF-TrFE) crystals to breakup ferroelectric domains, nanosized ferroelectric domains (or nanodomains) are obtained.[9, 20] As a result, relaxor ferroelectric behavior with high apparent dielectric constant (ε_r = 50-70) and low hysteresis loss (<20%) is observed for these P(VDF-TrFE-X) random terpolymers (X = CFE or CTFE). However, these terpolymers have low melting temperatures around 125 °C,

preventing high temperature applications. The second strategy is to graft linear dielectric polymer chains such as polystyrene[21-23] or polyacrylates[24-27] from P(VDF-CTFE)-based copolymers. At a low grafting density, these linear dielectric polymers segregate from the ferroelectric PVDF crystals, forming an insulating layer. Consequently, the normal ferroelectric behavior for PVDF gradually changes to double hysteresis loop behavior and finally to linear loops. Relatively high dielectric constants and thus high energy densities are achieved. The third strategy is to prepare PVDF-based block copolymers with microphase separated morphology.[28-29] By gradually decreasing the PVDF block content, double hysteresis or linear loops can be obtained with relatively high energy density.

Compared with chemical modification of PVDF and its random copolymers, polymer blends appear to be a much easier approach to suppress ferroelectricity in PVDF crystals. These blends can be either miscible [e.g., with poly(methyl methacrylate) (PMMA)] [30-32] or immiscible [e.g., with polycarbonate (PC)] blends, depending on favorable (e.g., dipole-dipole interactions between PMMA and PVDF) or unfavorable intermolecular interactions (e.g., incompatibility between bisphenol A moieties in PC and PVDF).[33] In this study, we investigated the morphological effect on dielectric properties of poly(VDF-*co*-hexafluoropropylene) [P(VDF-HFP)] blends (both miscible and immiscible) and multilayer films. For the miscible PMMA/P(VDF-HFP) blend films stretched to 400%, the PMMA content needed to be as high as 40 wt.% to suppress ferroelectric switching in PVDF crystals. Under such a high PMMA content, the crystallinity substantially decreased, thus deteriorating the mechanical property of the blend film. For immiscible PC/P(VDF-HFP) blend films, the PC content needed to reach at least 50 vol.% to suppress ferroelectric switching in PVDF crystals. On the other hand, for the immiscible PC/P(VDF-HFP) multilayer films, a PC content of only 30 vol.% was enough

to suppress ferroelectric switching in PVDF crystals. More importantly, the PC/P(VDF-HFP) multilayer films exhibited much higher breakdown strength than the blend films. It is clear that multilayer films exhibited significantly better dielectric properties than conventional blends, whether miscible or immiscible. Therefore, they are promising as next generation dielectric films for the electric storage application, aiming to achieve high temperature tolerance, high energy density, and low loss simultaneously.[34]

2. Experimental section

2.1. Materials

The P(VDF-HFP) random copolymer, Solef® 21508, was purchased from Solvay, and the HFP content was 15 wt.%. PMMA resin was purchased from Aldrich, and its weight-average molecular weight was 120000 Da. PC resin, Calibre™ 200-6, was purchased from Styron (now Trinseo). All resins were thoroughly dried under vacuum before melt processing.

2.2. Film preparation

PMMA/P(VDF-HFP) blends with different weight ratios (5/95, 10/90, 20/80, 30/70, and 40/60) were prepared using a Haake MiniLab II Micro Compounder at 200 °C for 15 min to ensure complete mixing. The extrudates were hot-pressed at 200 °C into ca. 30-40 μm films. The hot-pressed PMMA/P(VDF-HFP) blend films were uniaxially stretched using a home-built stretcher at room temperature up to a draw ratio of 400%.

PC/P(VDF-HFP) blend and multilayer films were prepared as reported before.[35] Briefly, the PC/P(VDF-HFP) blends with different volume fractions (10/90, 30/70, 50/50, 70/30, and 90/10) were compounded using a Haake twin-screw compounder, followed by extrusion to

produce ~12 μm thick films. PC/P(VDF-HFP) 32-layer films (~12 μm thick) with different volume fractions (10/90, 30/70, 50/50, 70/30, and 90/10) were produced using multilayer coextrusion at 260 °C, where the melt viscosities (at a shear rate of 10 s^{-1}) of PC and P(VDF-HFP) matched to ensure uniform layer thicknesses. Sacrificial low-density polyethylene (LDPE) surface layers were coextruded around the multilayer films to avoid any mechanical damage of multilayer films during melt-casting and film uptake. The sacrificial LDPE layers were removed before any tests of the multilayer films. For comparison purpose, control PMMA, PC, and P(VDF-HFP) films (ca. 10-12 μm thick) were also prepared via the melt coextrusion process.

2.3. Characterization methods and instrumentation

Thermal properties of all blend and multilayer films were measured using a Q2000 differential scanning calorimeter (DSC, TA Instruments). The instrument was calibrated with indium and tin standards. The heating and cooling rates were 10 °C/min and the sample weight was ca. 3 mg. Fourier transform infrared (FTIR) was carried out on a Nexus 870 FTIR ESP from Nicolet. The scanning range is from 4000 to 450 cm^{-1} with 32 scans at a resolution of 4 cm^{-1}.

Two-dimensional (2D) small-angle scattering (SAXS) and wide-angle X-ray diffraction (WAXD) patterns were collected at the X27C beamline of the National Synchrotron Light Source (NSLS), Brookhaven National Laboratory. The monochromatized X-ray wavelength was λ = 0.1371 nm. Either a Mar CCD detector or a Fujifilm imaging plate was used for SAXS and WAXD experiments. The distances between the sample and SAXS and WAXD detectors were calibrated using silver behenate with the first-order reflection at a scattering vector of q = 1.076 nm^{-1}. The data acquisition time for each SAXS or WAXD pattern was 30 s. Polar software (version 2.7.4, Stony Brook Technology and Applied Research, Inc., Stony Brook, NY) were used

to integrate the 2D patterns into 1D curves.

Morphology of the film samples were characterized using atomic force microscopy (AFM). Phase and height images of the cross-sections were recorded using a Nanoscope IIa Multimode scanning probe (Digital Instruments). AFM was operated using the tapping mode at room temperature.

Conventional BDS measurements were carried out on a Novocontrol Concept 80 broadband dielectric spectrometer to investigate the frequency- and temperature-dependent dielectric behavior for as-extruded and recrystallized multilayer films. After drying at 60 °C for 24 h, both sides of the film sample were coated with 20 nm thick gold as electrodes. The electrode diameter was 10 mm (area = 78.5 mm^2). For frequency-scan BDS measurements, real and imaginary relative permittivities (ε_r' and ε_r'') in the range of 10^{-2}–10^6 Hz were measured at a constant temperature.

D-E loops were measured using a Radiant Technology Premiere II ferroelectric tester at a frequency of 10 Hz with a sinusoidal wave function. Gold electrodes (20 nm thick) were sputter-coated on both sides of the film with a diameter of 2.5 mm. Samples were immersed in a silicone oil bath to avoid corona discharge in air. The maximum electric field was increased stepwise at an increment of 50 MV/m until breakdown of the film. High temperature tests were performed using an IKA RCT temperature controller. The discharged energy density and loss% could be calculated based on the D-E loop, following a previous report.[8]

Breakdown strength tests were conducted using a Quadtech (Marlborough, MA) Guardian 20 kV HiPot tester. An electrostatic sandwich setup was used for all breakdown measurements.[5] Film samples were masked using a thick, 100 μm Kapton® mask with a 1.5-cm diameter circular hole used to determine the sampling area. Two 1.2×6 cm^2 strips of 6 μm thick aluminum

metalized BOPP film were used as the flexible electrodes. The effective electrode area was thus 1.76 cm^2. The voltage was ramped at a speed of 50 $V \cdot s^{-1} \cdot \mu m^{-1}$ until electric breakdown. All measurements were conducted at room temperature in air. Breakdown data were recorded when the breakdown site was in the center area of the masked film (i.e., not via edge corona discharge).

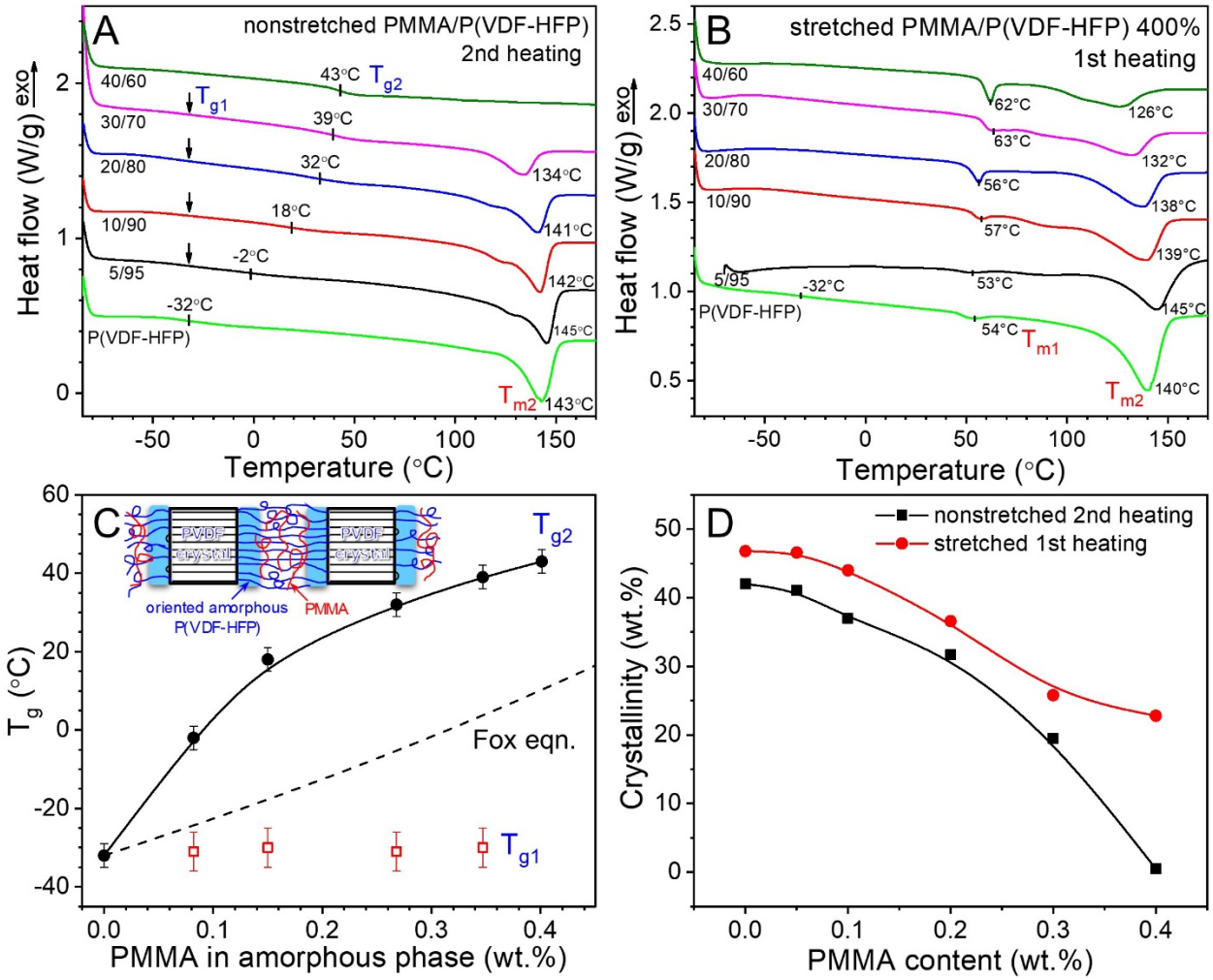

Fig. 1. (A) Second heating DSC curves for nonstretched PMMA/P(VDF-HFP) blend films and (B) first heating DSC curves for stretched (400% draw ratio) PMMA/P(VDF-HFP) blend films. (C) T_g as a function of PMMA wt.% in the amorphous phase for the nonstretched PMMA/P(VDF-HFP) blend films during second heating. (D) Crystallinity as a function of PMMA wt.% for nonstretched and stretched (400% draw ratio) PMMA/P(VDF-HFP) blend films.

3. Results and discussion

3.1. Crystalline structure and dielectric properties of miscible PMMA/P(VDF-HFP) blend films

It is well-known that PMMA is fully miscible with PVDF and its random copolymers as a result of strong dipole-dipole (or hydrogen-bonding like) interactions.[32, 36] PVDF and its random copolymers such as P(VDF-TrFE) and P(VDF-HFP) cannot be directly used as capacitor films because of their significant ferroelectricity.[9, 16-17] By blending PMMA into PVDF and its random copolymers, it is possible to reduce the crystallite size and minimize ferroelectric switching in PVDF crystals.[37-40] In this study, we evaluated this approach at the film level for capacitor applications. Before dielectric property characterization, the effect of PMMA incorporation on the crystalline structure and morphology of P(VDF-HFP) was studied, especially for uniaxially stretched blend films up to a draw ratio of 400%.

Fig. 1A shows the second heating DSC curves for nonstretched PMMA/P(VDF-HFP) blend films with different PMMA weight contents. With addition of PMMA up to 40 wt.%, the T_g (i.e., T_{g2}) gradually increased. These T_{g2} values were significantly higher than those predicted by the Fox equation,[41] as shown in Fig. 1C. In addition to T_{g2}, there existed another weak T_g around -30 °C (i.e., T_{g1}) in DSC. Although it was faint in DSC, this T_g was quite obvious in BDS and dynamic mechanical analysis (DMA), as reported before.[30, 41-42] This T_g did not change much upon increasing the PMMA content. The T_{g1} was explained by the oriented amorphous chains stemming out of the PVDF lamellar crystals [i.e., the oriented amorphous fraction (OAF); see the inset scheme in Fig. 1C].[15] Due to the relatively tight packing of the OAF, no PMMA chains could enter this region and thus T_{g1} kept around -30 °C, which was similar to that for neat P(VDF-HFP).[30, 41-42] Currently, the percentage of the OAF could not be accurately determined for the nonstretched blends. If correcting the PMMA content in the truly mixed

amorphous phase using the OAF percentage , the T_{g2} values should get closer to the Fox prediction. Upon addition of PMMA, the melting temperature (i.e., T_{m2}) became gradually lower whereas the crystallinity decreased drastically (Fig. 1D). Finally, with 40 wt.% PMMA, the nonstretched blend film became completely amorphous.

After 400% uniaxial stretching, the T_{m2} slightly decreased compared to the nonstretched films, because mechanical stretching decreased the crystallite size. Nonetheless, the overall crystallinity increased, possibly due to strain-induced crystallization (Fig. 1D). In particular, the stretched 40 wt.% PMMA blend film had a crystallinity of 22 wt.%. Upon the first heating, a weak T_{m1} around 60 °C was observed for all films. This could be attributed to the melting of secondary crystals formed during mechanical stretching, as we reported before.[15, 43]

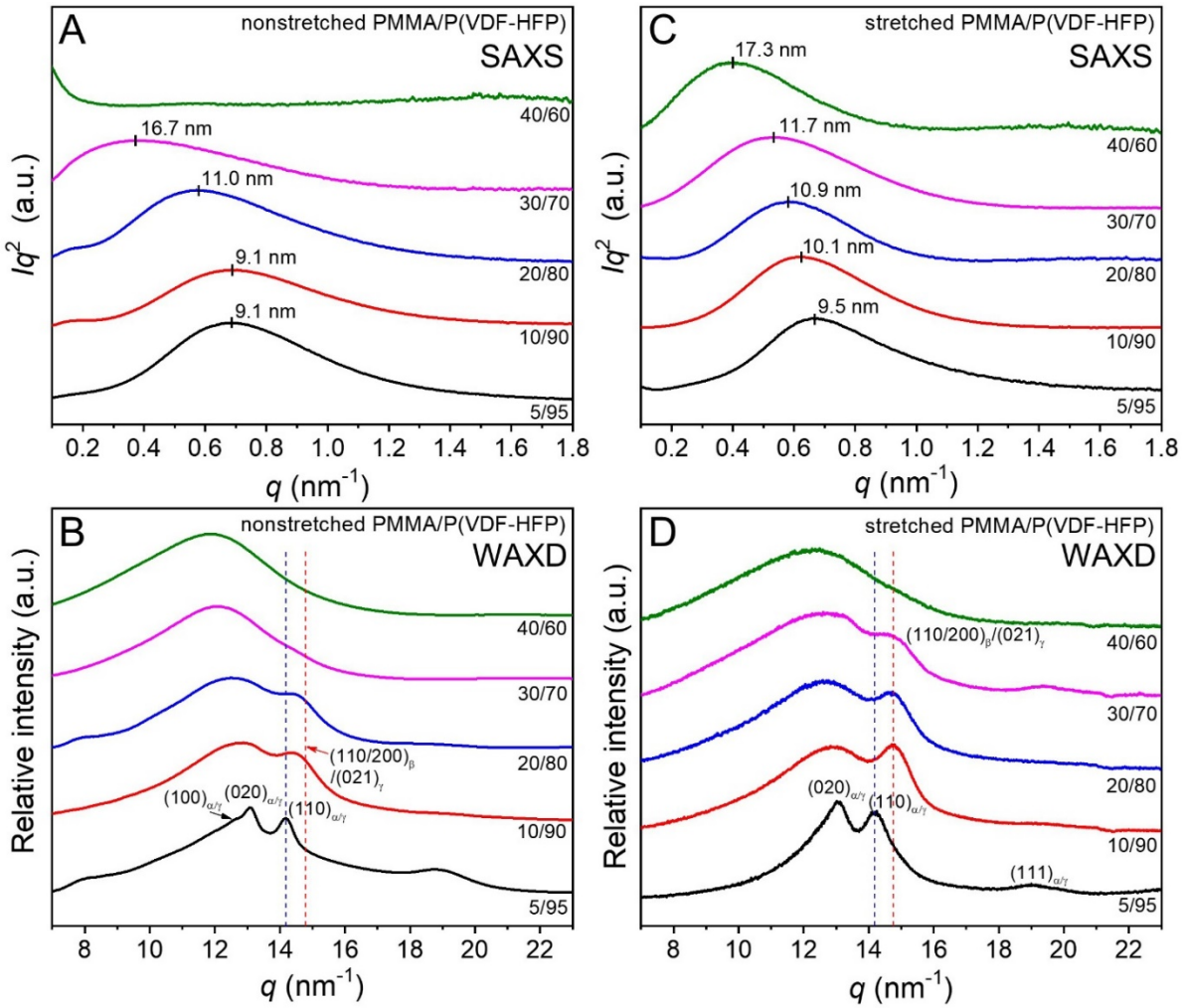

Fig. 2. (A,C) SAXS profiles and (B,D) WAXD profiles for (A,B) nonstretched and (C,D) stretched (draw ratio at 400%) PMMA/P(VDF-HFP) blend films.

The crystalline polymorphism in these PMMA/P(VDF-HFP) blend films were first studied by WAXD. The lamellar structure was studied by SAXS. The corresponding 2D SAXS and WAXD patterns are shown in Fig. S1 in the Supplementary Information. Figs. 2A and B show 1D SAXS profiles for nonstretched and stretched PMMA/P(VDF-HFP) blend films, respectively. Upon increasing the PMMA content, the lamellar *d*-spacing gradually became larger. This could be primarily attributed to the thickening of the amorphous layers sandwiched between neighboring lamellae.

From Fig. 2C, the nonstretched 5/95 blend film was primarily in the α crystalline form.

The (110) reflection for the nonstretched 10/90, 20/80, and 30/70 blend films shifted to a higher *q* value, suggesting the appearance of certain γ or β crystalline form upon addition of PMMA in P(VDF-HFP). Finally, the nonstretched 40/60 blend film became completely amorphous. From Fig. 2D, the stretched blend films exhibited higher crystallinities. The stretched 5/95 blend film exhibited mostly the α form. For other stretched blend films with higher PMMA contents, the β form was clearly observed. This result suggested that both addition of PMMA and uniaxial stretching favored the formation of polar β form in P(VDF-HFP).

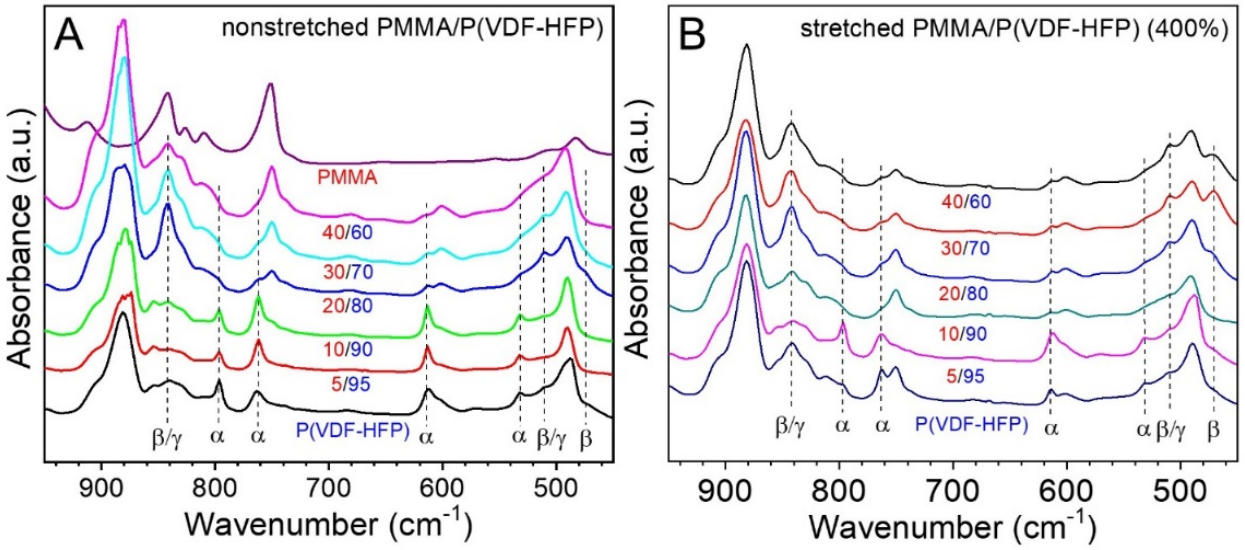

Fig. 3. FTIR spectra for (A) nonstretched and (B) stretched (400%) PMMA/P(VDF-HFP) blend films. The spectra of control PMMA and P(VDF-HFP) (both nonstretched and stretched) films are included for comparison.

The polymorphism in nonstretched and stretched PMMA/P(VDF-HFP) blend films was further confirmed by FTIR, as shown in Fig. 3. For nonstretched PMMA/P(VDF-HFP) blend films (Fig. 3A), the α form was the major component for the 5/95 and 10/90 blend films, because the β/γ peak at 840 cm^{-1} was absent. For the nonstretched 20/80 and 30/70 blend films, the β/γ peak at 840 cm^{-1} appeared whereas the α peaks at 795, 760, 614, and 532 cm^{-1} disappeared, indicating that the formation of the β/γ form was induced by PMMA. For the nonstretched 40/60

blend film, the 840 cm^{-1} peak became weaker. From DSC and WAXD results, this blend film was fully amorphous.

For the stretched PMMA/P(VDF-HFP) blend films in Fig. 3B, only the 5/95 film showed the presence of the α form, indicated by the α peaks at 795, 760, 714, and 532 cm^{-1}. For the rest stretched blend films, the β/γ peak at 840 cm^{-1} became obvious, indicating the formation of the β form upon addition of PMMA and mechanical stretching.

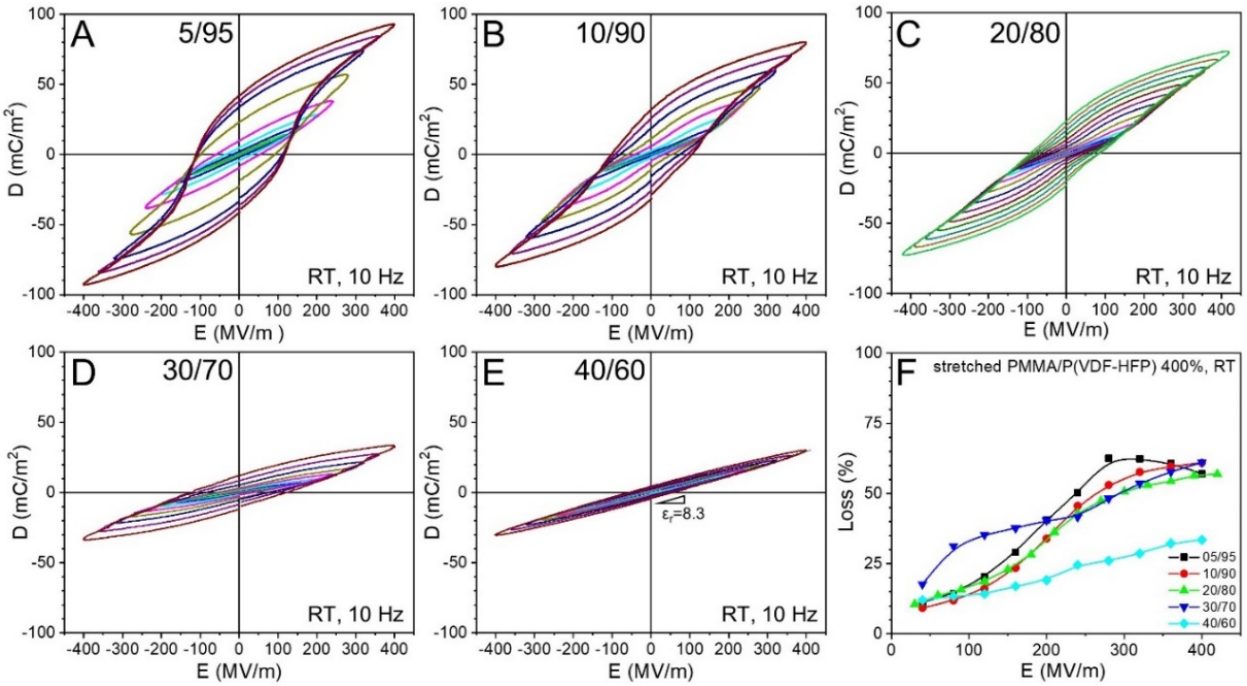

Fig. 4. Bipolar D-E loops for PC/P(VDF-HFP) blend films: (A) 10/90, (B) 30/70, (C) 50/50, (D) 70/30, and (E) 90/10 (vol./vol.) at room temperature. The poling frequency was 10 Hz with a sinusoidal wave function. (F) shows loss% as a function of electric field for different blend films.

High-field ferroelectric properties were studied by D-E loop tests on stretched PMMA/P(VDF-HFP) blend films. The effects of different draw ratios on crystalline morphology and ferroelectric properties for the PMMA/P(VDF-HFP) 20/80 blend film are shown in Fig. S2. Upon increasing the draw ratio, more and more oriented PVDF crystals were observed in both 2D SAXS and WAXD patterns. This was reflected by an increase of the Herman's orientation factor,

f, from 0.05 for the nonstretched film to 0.86 for the 400% stretched film. Meanwhile, for the nonstretched film, linear D-E loops were seen when the poling field was up to 225 MV/m. Upon increasing the draw ratio, double hysteresis loops developed with gradually enhanced maximum polarization. This was attributed to the crystal orientation effect,[23] because VDF dipoles could respond more readily in oriented films than the nonstretched films with a random crystal orientation. For this study, we used 400% stretched blend films for the high-field dielectric property study.

Fig. 4 shows bipolar D-E loops for 400% stretched PMMA/P(VDF-HFP) blend films with different PMMA contents. The poling was performed at room temperature with a sinusoidal wave function at 10 Hz. For the 5/95 and 10/90 blend films, typical ferroelectric loops were seen. This could be attributed to the fact that PMMA did not decrease the PVDF crystallinity much for both films, as seen in Fig. 1D. For the 20/80 blend film, double hysteresis loops were observed. For the 30/70 blend film, limited ferroelectric switching was observed only when the poling field was above 200 MV/m. Finally, for the 40/60 blend film, linear D-E loops were obtained even when the poling field was as high as 400 MV/m. This could be attributed to nonuniform electric field distribution in the amorphous and crystalline phases of the blend films. For a multiphase dielectric under a high applied electric field, the low dielectric constant phase [i.e., the amorphous PMMA/P(VDF-HFP) phase] bears a high local electric field, and the high dielectric constant phase (the PVDF crystalline phase) should have a low local electric field.[9, 44-45] It is likely that at a high PMMA content, the local electric field in PVDF crystals became too weak to induce any ferroelectric switching of ferroelectric domains. From these bipolar D-E loops, the energy loss% could be calculated, and results are summarized in Fig. 4F. When the PMMA content was below 30 wt.%, significant loss% values (around 50%) were observed when then poling electric field was

above 250 MV/m. Only for the 40/60 blend film, the loss% remained the lowest among all samples.

Similar D-E loops were observed for these miscible blend films at 50 (Fig. S3) and 75 °C (Fig. S4), respectively. Meanwhile, the hysteresis loss% increased upon increasing temperature (see Figs. S3F and S4F). From this study, we conclude that blending a miscible polymer such as PMMA with PVDF was not effective in suppressing the ferroelectric switching behavior for PVDF, unless the content of PMMA reached very high (e.g., 40 wt.%). However, this miscible blend approach is not practical because too much PMMA significantly decreased the crystallinity and thus decreased mechanical strength for the blend films.

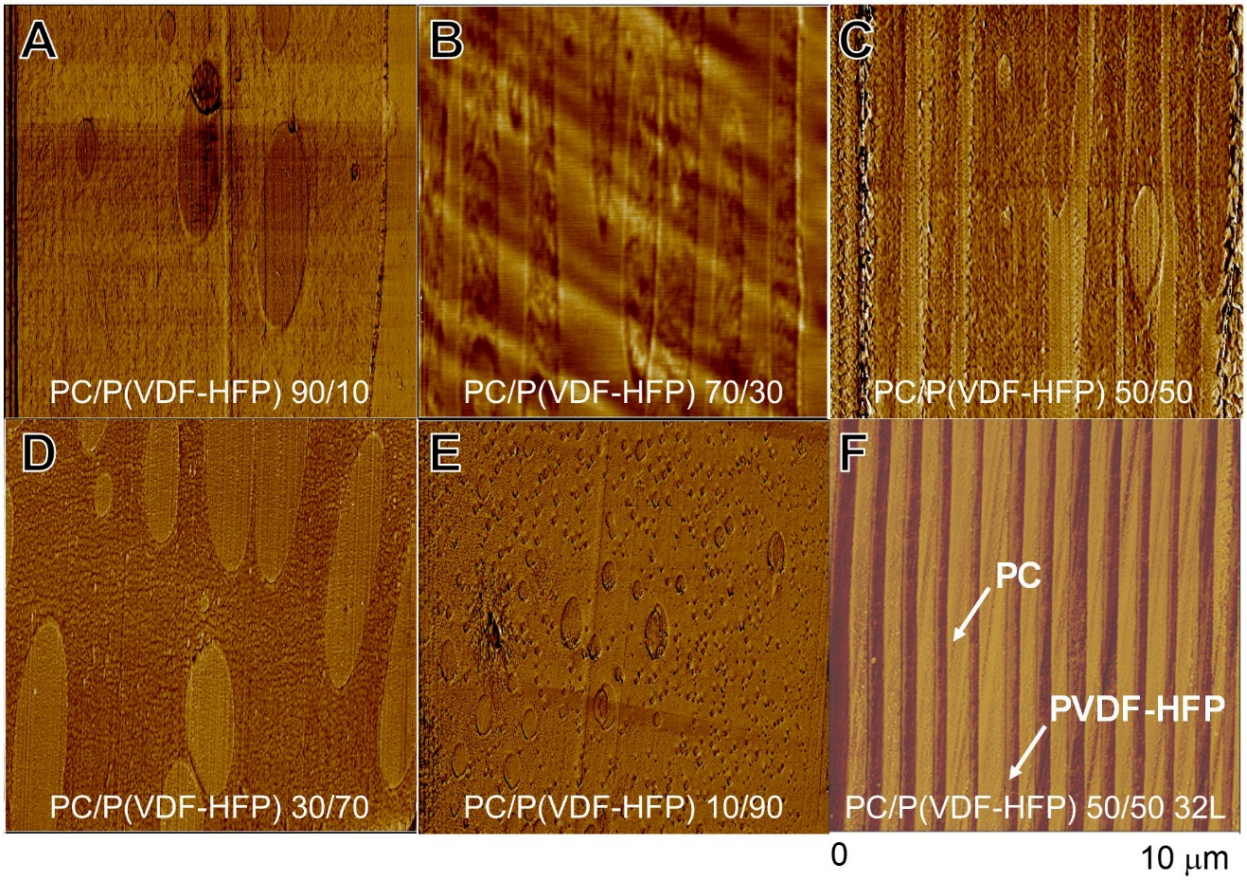

Fig. 5. Cross-section AFM phase images for PC/P(VDF-HFP) blend films: (A) 90/10, (B) 70/30, (C) 50/50, (D) 30/70, and (E) 10/90. (F) shows the cross-section of the PC/P(VDF-HFP) 50/50 32L film.

3.2. Morphology and dielectric behavior for immiscible PC/P(VDF-HFP) blend and multilayer films

If the miscible blend approach is not viable, how about the immiscible blend approach? In this study, we continued to study two different immiscible polymer blend films, namely, conventional blend and coextruded multilayer films.[46] Figs. 5A-E show AFM phase images of the cross-sections of PC/P(VDF-HFP) blend films with different compositions. It can be seen when PVDF was the minority component such as in PC/P(VDF-HFP) 90/10 (Fig. 5A) and 70/30 (Fig. 5B) blend films, PVDF formed the islands in the PC matrix. When PC was the minority component such as in PC/P(VDF-HFP) 30/70 (Fig. 5D) and 10/90 (Fig. 5E) blend films, PC formed the islands in the PVDF matrix. When the composition was 50/50, bicontinuous morphology was formed (Fig. 5C). Since all blends were extruded into ca. 12 μm films, the microdomains became anisotropic in the thickness direction. Using the forced coextrusion technology, PC/P(VDF-HFP) multilayer films were obtained.[35] An example AFM phase image is shown in Fig. 5F for PC/P(VDF-HFP) 50/50 32-layer (32L) film. Relatively uniform PC and P(VDF-HFP) layers were observed. In these images, PC had a higher modulus than P(VDF-HFP). Therefore, PC microdomains/layers appeared brighter and PVDF microdomains/layers appeared darker.

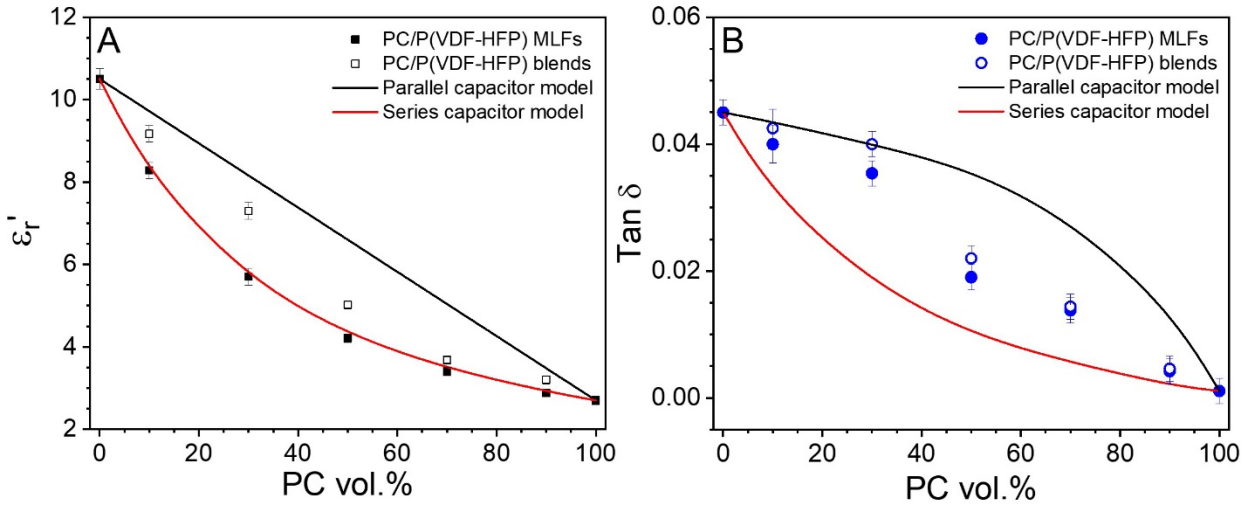

Fig. 6. (A) Dielectric constant as a function of PC vol.% for PC/P(VDF-HFP) blend and multilayer films. (B) Dissipation factor (tanδ) as a function of PC vol.%. Theoretical predictions for parallel and series capacitor models are shown for comparison.

Because PC has poor uniaxial or biaxial stretchability, we could not stretch PC/P(VDF-HFP) blend and multilayer films. In addition, PVDF crystals adopted the edge-on crystal orientation when confined in the sub-micron scale space.[47] The frequency-scan BDS results for the PC/P(VDF-HFP) blend and multilayer films at 25, 50, and 75 °C are shown in Figs. S5 and S6, respectively. From these results, dielectric constant (ε_r') and tanδ as a function of PC vol.% can be obtained, as seen in Figs. 6A and B, respectively. In both figures, predictions from both parallel and series capacitor models are shown. Derivation of ε_r', ε_r'', and tanδ for parallel and series capacitor models are described in Section V in the Supplementary Information. Compared with parallel and series capacitor models, the multilayer film ε_r' fit the series model very well and the blend film ε_r' were between the predictions of the parallel and series capacitor models (Fig. 6A). This is understandable because immiscible blends could not be represented by the parallel model (see morphology in Fig. 5). The tanδ values for the multilayer films appeared to be higher than the series model predictions. Note that derivation of tanδ in Section V of the Supplementary Information ignored any conduction of space charges or impurity ions in the samples. If there

was certain conduction of impurity ions in the multilayer films, the overall tanδ would be greater than those predicted by the series capacitor model. For the immiscible blend films, tanδ were lower than the parallel model prediction at high PC contents. At low PC contents, the tanδ values fit well with the parallel model prediction.

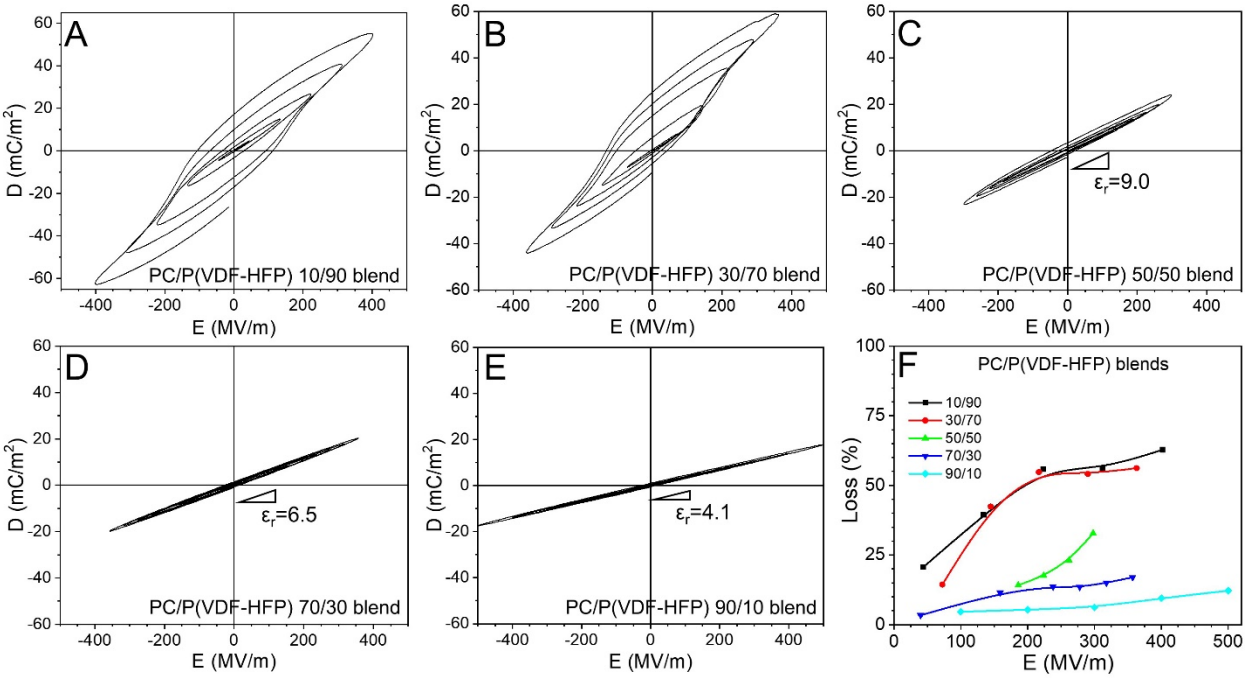

Fig. 7. Bipolar D-E loops for PC/P(VDF-HFP) blend films: (A) 10/90, (B) 30/70, (C) 50/50, (D) 70/30, and (E) 90/10 (vol./vol.) at room temperature. The poling frequency was 10 Hz with a sinusoidal wave function. (F) shows loss% as a function of electric field for different blend films.

High-field ferroelectric behavior for the PC/P(VDF-HFP) blend films was studied by five continuous D-E loops, as shown in Fig. 7. For PC/P(VDF-HFP) 10/90 and 30/70 blend films, typical ferroelectric loops were seen. When the PC content was 50 vol.% or below, linear D-E loops were obtained, and the ε_r decreases upon increasing the PC vol.%. The energy loss% is shown in Fig. 7F. When the PC content was below 30 vol.%, ferroelectric switching led to significant loss. When the PC content was 50 vol.%, the loss% was relatively high when the poling field was above 200 MV/m. Only when the PC content was higher than 70 vol.%, the

loss% remained reasonably low. However, the low ε_r for the blend films of high PC contents was disadvantages.

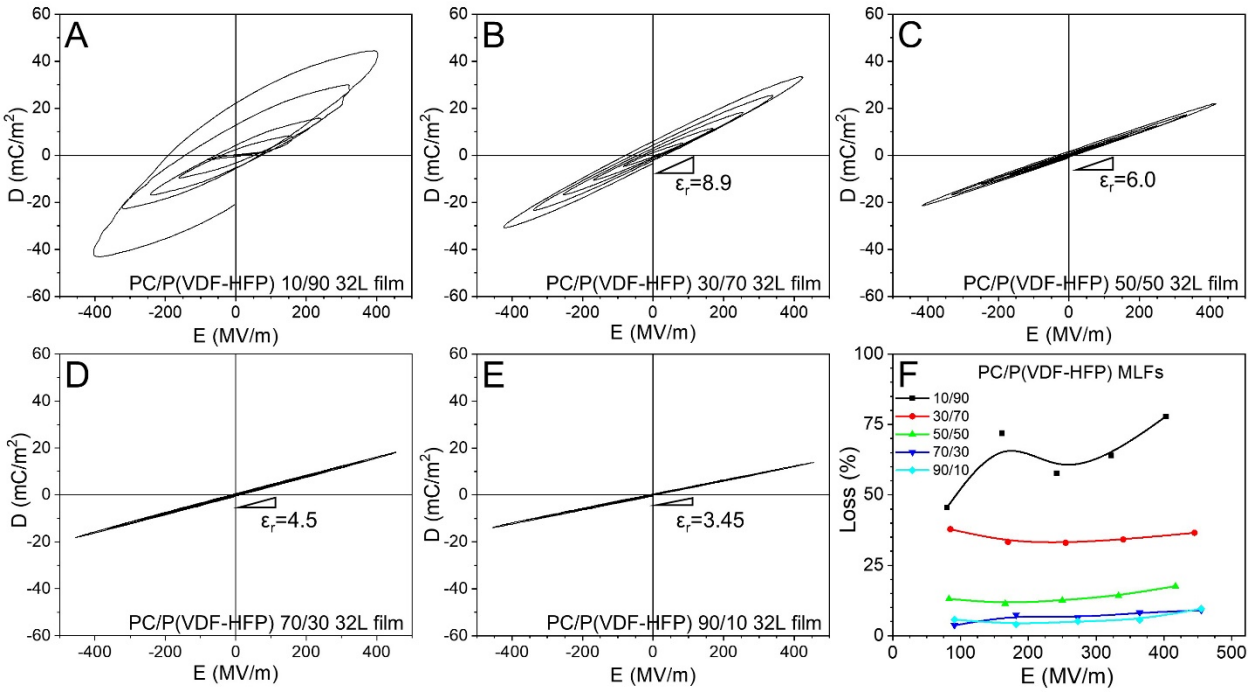

Fig. 8. Bipolar D-E loops for PC/P(VDF-HFP) multilayer films: (A) 10/90, (B) 30/70, (C) 50/50, (D) 70/30, and (E) 90/10 (vol./vol.) at room temperature. The poling frequency was 10 Hz with a sinusoidal wave function. (F) shows loss% as a function of electric field for different multilayer films.

For PC/P(VDF-HFP) multilayer films, the situation changed. Only for the PC/P(VDF-HFP) 10/90 32L film, ferroelectric switching was observed. For the multilayer films with PC content greater than 30 vol.%, linear D-E loops were observed and they were slimmer than those of the blend films at the same PC content. Upon increasing the PC content, the ε_r gradually decreased. The energy loss% values are shown in Fig. 8F. The PC/P(VDF-HFP) 10/90 film exhibited high loss% due to ferroelectric switching. Multilayer films exhibited reasonably low loss% when the PC content was higher than 50 vol.%.

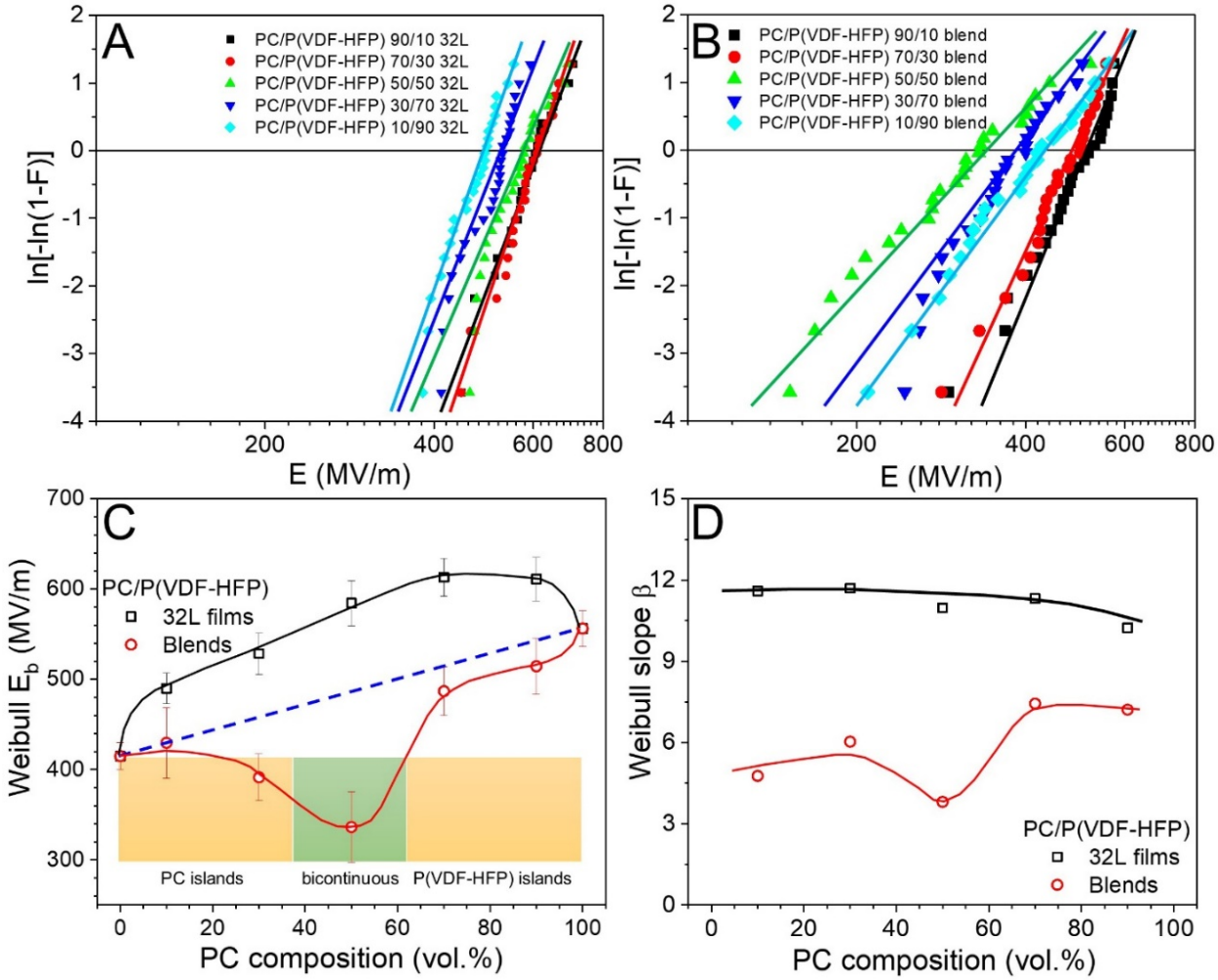

Fig. 9. Weibull breakdown analyses for PC/P(VDF-HFP) (A) blend and (B) multilayer films at room temperature. (C) Weibull breakdown strength at 63.2% failure probability and (D) Weibull slope β as a function of PC vol.% for PC/P(VDF-HFP) blend and multilayer films.

The dielectric breakdown strength for the immiscible blend and multilayer films were studied using Weibull analysis. From the Weibull plots in Fig. 9, both breakdown strength (E_b) at 63.2% failure probability (Fig. 9A) and slope β (Fig. 9B) could be obtained. From Fig. 9A, it is intriguing to see that PC/P(VDF-HFP) multilayer films exhibited higher E_b than the linear average, whereas the blend films showed lower E_b than the linear average. The minimum E_b was observed for the 50/50 blend film. This is understandable because the 50/50 blend film exhibited bicontinuous morphology (Fig. 5C) and all other blend films exhibit the island-in-the-sea

morphology. We consider that the bicontinuous PC/P(VDF-HFP) interfaces must have helped the conduction of hot electrons injected from the metal electrodes under a high poling field, especially when they happen to orient parallel to the external electric field. From Fig. 9B, the Weibull slope β values for the multilayer films were higher than those of the blend films. From this breakdown study, we conclude that multilayer films with the PC content greater than 50 vol.% should be more advantageous than the blend films, because they have higher E_b and β values. This could be attributed to the perpendicular PC/P(VDF-HFP) interfaces, which serve as effective blockage for injected hot electrons from the metal electrodes, as we reported recently.[48-49]

4. Conclusions

As we know, PVDF and its random copolymers are ferroelectric, which significantly hampers its application for film capacitors. Therefore, modification of PVDF and its random copolymers is highly desired to suppress the ferroelectricity (i.e., nonlinear dielectric property [50]). Polymer blend appears to be an easier approach than synthesis of block or graft PVDF copolymers for this purpose. In this study, we have examined both miscible (PMMA) and immiscible (PC) blends with P(VDF-HFP). First, when the PMMA content was ≤30 wt.%, 400% stretched PMMA/P(VDF-HFP) blend films still exhibited significant ferroelectric switching. When the PMMA content reached 40 wt.%, linear D-E loops were achieved; however, the PVDF crystallinity dramatically dropped and the mechanical property became poor. Second, we studied immiscible PC/P(VDF-HFP) blends and multilayer films. Due to the immiscibility, P(VDF-HFP) could still crystallize at all compositions to keep good mechanical property. When the PC content was ≥50 vol.%, linear D-E loops were obtained for the blend films. However, the hysteresis loss% was still quite high. For PC/P(VDF-HFP) multilayer films, linear D-E loops could be obtained

at a lower PC content of only 30 vol.%. More importantly, the PC/P(VDF-HFP) blend films exhibited significantly lower breakdown strength than the multilayer films, especially at the 50/50 composition with a bicontinuous morphology. This could be attributed to the more conductive pathway along the interfaces in the bicontinuous blend film. On the contrary, PC/P(VDF-HFP) multilayer films exhibited higher breakdown strength than the linear average values, because all interfaces were perpendicular to the applied electric field. As such, interfacial polarization significantly prevented the thermal runaway of hot electrons injected from the metal electrode, as we reported recently.[48-49] Compared with both miscible and immiscible polymer blends, multilayer film is a viable approach to realize relatively high dielectric constant, high energy storage, high breakdown strength, and low dielectric loss simultaneously.

Author information

Corresponding Author

*E-mail: (L. Zhu) lxz121@case.edu.

Notes

The authors declare no competing financial interest.

Acknowledgements

This work on immiscible PC/P(VDF-HFP) blend and multilayer films was supported by National Science Foundation via the Partnerships for Innovation: Building Innovation Capacity Program (IIP-1237708). The study on miscible PMMA/P(VDF-HFP) blends was supported by Office of Naval Research (N00014-16-1-2170). The synchrotron X-ray study carried out at NSLS was supported by Department of Energy, Office of Science.

Appendix A. Supplementary data

Supplementary data related to this article can be found at xxxxxxxxxxxxxxxxxxxxx.

References

[1] I. Husain. Electric and Hybrid Vehicles: Design Fundamentals. Boca Raton: CRC Press, 2010.

[2] W.J. Sarjeant. Capacitors, IEEE Trans. Electr. Insul. 25 (1990) 861-922.

[3] W.J. Sarjeant, J. Zirnheld, F.W. MacDougall. Capacitors, IEEE Trans. Plasm. Sci. 26 (1998) 1368-1392.

[4] J. Ho, R. Ramprasad, S. Boggs. Effect of alteration of antioxidant by UV treatment on the dielectric strength of BOPP capacitor film, IEEE Trans. Dielectr. Electr. Insul. 14 (2007) 1295-1301.

[5] J. Ho, T.R. Jow. Characterization of high temperature polymer thin films for power conditioning capacitors. Adelphi, MD: Army Research Laboratory, 2009.

[6] J. Ho, T.R. Jow. High field conduction in biaxially oriented polypropylene at elevated temperature, IEEE Trans. Dielectr. Electr. Insul. 19 (2012) 990-995.

[7] D. Montanari, K. Saarinen, F. Scagliarini, D. Zeidler, M. Niskala,C. Nender. Film capacitors for automotive and industrial applications. Proceedings of CARTS U.S.A. 2009, Jacksonville, FL, March 30-April 2, 2009.

[8] L. Zhu, Q. Wang. Novel ferroelectric polymers for high energy density and low loss dielectrics, Macromolecules 45 (2012) 2937-2954.

[9] L. Zhu. Exploring strategies for high dielectric constant and low loss polymer dielectrics,

J. Phys. Chem. Lett. 5 (2014) 3677-3687.

[10] Q. Chen, Y. Shen, S. Zhang, Q.M. Zhang. Polymer-based dielectrics with high energy storage density, Annu. Rev. Mater. Res. 45 (2015) 433-458.

[11] Prateek, V.K. Thakur, R.K. Gupta. Recent progress on ferroelectric polymer-based nanocomposites for high energy density capacitors: Synthesis, dielectric properties, and future aspects, Chem. Rev. 116 (2016) 4260-4317.

[12] Q. Li, F.Z. Yao, Y. Liu, G.Z. Zhang, H. Wang, Q. Wang. High-temperature dielectric materials for electrical energy storage, Ann. Rev. Mater. Res. 48 (2018) 219-243.

[13] R. Gregorio Jr., E.M. Ueno. Effect of crystalline phase, orientation and temperature on the dielectric properties of poly (vinylidene fluoride) (PVDF), J. Mater. Sci. Lett. 34 (1999) 4489-4500.

[14] F. Guan, J. Pan, J. Wang, Q. Wang, L. Zhu. Crystal orientation effect on electric energy storage in poly(vinylidene fluoride-*co*-hexafluoropropylen) copolymers, Macromolecules 43 (2010) 384-392.

[15] L. Yang, J. Ho, E. Allahyarov, R. Mu, L. Zhu. Semicrystalline structure dielectric property relationship and electrical conduction in a biaxially oriented poly(vinylidene fluoride) film under high electric fields and high temperatures, ACS Appl. Mater. Interfaces 7 (2015) 19894-19905.

[16] A.J. Lovinger. Ferroelectric polymers, Science 220 (1983) 1115-1121.

[17] H.S. Nalwa. Ferroelectric Polymers: Chemistry, Physics, and Applications. New York: Marcel Dekker, 1995.

[18] T.C. Chung, A. Petchsuk. Synthesis and properties of ferroelectric fluoroterpolymers with Curie transition at ambient temperature, Macromolecules 35 (2002) 7678-7684.

[19] F. Xia, Z. Cheng, H. Xu, H. Li, Q. Zhang, G.J. Kavarnos, R.Y. Ting, G. Abdul-Sadek, K.D. Belfield. High electromechanical responses in a poly(vinylidene fluoride-trifluoroethylene-chlorofluoroethylene) terpolymer, Adv. Mater. 14 (2002) 1574-1577.

[20] L. Yang, X. Li, E. Allahyarov, P.L. Taylor, Q.M. Zhang, L. Zhu. Novel polymer ferroelectric behavior via crystal isomorphism and the nanoconfinement effect, Polymer 54 (2013) 1709-1728.

[21] F. Guan, J. Wang, L. Yang, J.-K. Tseng, K. Han, Q. Wang, L. Zhu. Confinement-induced high-field antiferroelectric-like behavior in a poly(vinylidene fluoride-*co*-trifluoroethylene-*co*-chlorotrifluoroethylene)-*graft*-polystyrene graft copolymer, Macromolecules 44 (2011) 2190-2199.

[22] F. Guan, L. Yang, J. Wang, B. Guan, K. Han, Q. Wang, L. Zhu. Confined ferroelectric properties in poly(vinylidene fluoride-*co*-chlorotrifluoroethylene)-*graft*-polystyrene graft copolymers for electric energy storage applications, Adv. Funct. Mater. 21 (2011) 3176-3188.

[23] L. Yang, E. Allahyarov, F. Guan, L. Zhu. Crystal orientation and temperature effects on double hysteresis loop behavior in a poly(vinylidene fluoride-*co*-trifluoroethylene-*co*-chlorotrifluoroethylene)-*graft*-polystyrene graft copolymer, Macromolecules 46 (2013) 9698-9711.

[24] J. Li, S. Tan, S. Ding, H. Li, L. Yang, Z. Zhang. High-field antiferroelectric behaviour and minimized energy loss in poly(vinylidene-*co*-trifiuoroethylene)-*graft*-poly(ethyl methacrylate) for energy storage application, J. Mater. Chem. 22 (2012) 23468-23476.

[25] J. Li, X. Hu, G. Gao, S. Ding, H.Y. Li, L. Yang, Z. Zhang. Tuning phase transition and ferroelectric properties of poly(vinylidene fluoride-*co*-trifluoroethylene) via grafting with

desired poly(methacrylic ester)s as side chains, J. Mater. Chem. C 1 (2013) 1111-1121.

[26] J. Li, H. Gong, Q. Yang, Y. Xie, L. Yang, Z. Zhang. Linear-like dielectric behavior and low energy loss achieved in poly(ethyl methacrylate) modified poly(vinylidene-*co*-trifluoroethylene), Appl. Phys. Lett. 104 (2014) 263901.

[27] H.H. Gong, B. Miao, X. Zhang, J.Y. Lu, Z.C. Zhang. High-field antiferroelectric-like behavior in uniaxially stretched poly(vinylidene fluoride-trifluoroethylene-chlorotrifluoroethylene)-grafted-poly(methyl methacrylate) films with high energy density, RSC Adv. 6 (2016) 1589-1599.

[28] V.S.D. Voet, G. ten Brinke, K. Loos. Well-defined copolymers based on poly(vinylidene fluoride): From preparation and phase separation to application, J. Polym. Sci., Part A: Polym. Chem. 52 (2014) 2861-2877.

[29] I. Terzic, N.L. Meereboer, M. Acuautla, G. Portale, K. Loos. Tailored self-assembled ferroelectric polymer nanostructures with tunable response, Macromolecules 52 (2019) 354-364.

[30] B.R. Hahn, O. Herrmannschonherr, J.H. Wendorff. Evidence for a crystal-amorphous interphase in PVDF and PVDF/PMMA blends, Polymer 28 (1987) 201-208.

[31] J. Mijovic, J.W. Sy, T.K. Kwei. Reorientational dynamics of dipoles in poly(vinylidene fluoride) poly(methyl methacrylate) (PVDF/PMMA) blends by dielectric spectroscopy, Macromolecules 30 (1997) 3042-3050.

[32] M.Y. Li, N. Stingelin, J.J. Michels, M.J. Spijkman, K. Asadi, K. Feldman, P.W.M. Blom, D.M. de Leeuw. Ferroelectric phase diagram of PVDF:PMMA, Macromolecules 45 (2012) 7477-7485.

[33] X.J. Zhao, G.R. Peng, Z.J. Zhan. Dielectric and energy storage properties of the

heterogeneous P(VDF-HFP)/PC composite films, JOM 69 (2017) 2453-2459.

[34] E. Baer, L. Zhu. 50th Anniversary perspective: Dielectric phenomena in polymers and multilayered dielectric films, Macromolecules 50 (2017) 2239-2256.

[35] M. Mackey, A. Hiltner, E. Baer, L. Flandin, M.A. Wolak, J.S. Shirk. Enhanced breakdown strength of multilayered films fabricated by forced assembly microlayer coextrusion, J. Phys. D-Appl. Phys. 42 (2009) 175304.

[36] G. Zhong, L. Zhang, R. Su, K. Wang, H. Fong, L. Zhu. Understanding polymorphism formation in electrospun fibers of immiscible Poly(vinylidene fluoride) blends, Polymer 52 (2011) 2228-2237.

[37] Q.J. Meng, W.J. Li, Y.S. Zheng, Z.C. Zhang. Effect of poly(methyl methacrylate) addition on the dielectric and energy storage properties of poly(vinylidene fluoride), J. Appl. Polym. Sci. 116 (2010) 2674-2684.

[38] W.M. Xia, Q.P. Zhang, X. Wang, Z.C. Zhang. Electrical energy discharging performance of poly(vinylidene fluoride-*co*-trifluoroethylene) by tuning its ferroelectric relaxation with polymethyl methacrylate, J. Appl. Polym. Sci. 131 (2014) 40114.

[39] B.C. Luo, X.H. Wang, H.X. Wang, Z.M. Cai, L.T. Li. P(VDF-HFP)/PMMA flexible composite films with enhanced energy storage density and efficiency, Compos. Sci. Technol. 151 (2017) 94-103.

[40] G.R. Peng, X.J. Zhao, Z.J. Zhan, S.Z. Ci, Q. Wang, Y.J. Liang, M.L. Zhao. New crystal structure and discharge efficiency of poly(vinylidene fluoride-hexafluoropropylene)/poly(methyl methacrylate) blend films, RSC Adv. 4 (2014) 16849-16854.

[41] B. Lu, K. Lamnawar, A. Maazouz, H.G. Zhang. Revealing the dynamic heterogeneity of

PMMA/PVDF blends: from microscopic dynamics to macroscopic properties, Soft Matter 12 (2016) 3252-3264.

[42] B. Hahn, J. Wendorff, D.Y. Yoon. Dielectric relaxation of the crystal-amorphous interphase in poly(vinylidene fluoride) and its blends with poly(methyl methacrylate), Macromolecules 18 (1985) 718-721.

[43] H. Huang, X. Chen, R. Li, M. Fukuto, D.E. Schuele, M. Ponting, D. Langhe, E. Baer, L. Zhu. Flat-on secondmary crystals as effective blocks to reduce ionic conduction loss in polysulfone/poly(vinylidene fluoride) multilayer dielectric films, Macromolecules 51 (2018) 5019-5026.

[44] M. Mackey, D.E. Schuele, L. Zhu, L. Flandin, M.A. Wolak, J.S. Shirk, A. Hiltner, E. Baer. Reduction of dielectric hysteresis in multilayered films via nanoconfinement, Macromolecules 45 (2012) 1954-1962.

[45] K.-C. Kao. Dielectric Phenomena in Solids: with Emphasis on Physical Concepts of Electronic Processes. Boston: Elsevier Academic Press, 2004.

[46] D. Langhe, M. Ponting. Manufacturing and Novel Applications of Multilayer Polymer Films. Amsterdam: Elsevier, 2015.

[47] M. Mackey, L. Flandin, A. Hiltner, E. Baer. Confined crystallization of PVDF and a PVDF-TFE copolymer in nanolayered films, J. Polym. Sci., Part B: Polym. Phys. 49 (2011) 1750-1761.

[48] J.K. Tseng, S. Tang, Z. Zhou, M. Mackey, J.M. Carr, R. Mu, L. Flandin, D.E. Schuele, E. Baer, L. Zhu. Interfacial polarization and layer thickness effect on electrical insulation in multilayered polysulfone/poly(vinylidene fluoride) films, Polymer 55 (2014) 8-14.

[49] X. Chen, J.-K. Tseng, I. Treufeld, M. Mackey, D.E. Schuele, R. Li, M. Fukuto, E. Baer, L.

Zhu. Enhanced dielectric properties due to space charge-induced interfacial polarization in multilayer polymer films, J. Mater. Chem. C 5 (2017) 10417-10426.

[50] Y. Li, J. Ho, J. Wang, Z.-M. Li, G.-J. Zhong, L. Zhu. Understanding nonlinear dielectric properties in a biaxially oriented poly(vinylidene fluoride) film at both low and high electric fields, ACS Appl. Mater. Interfaces 8 (2016) 455-465.

Supplementary Information

Morphological effects on dielectric properties of poly(vinylidene fluoride-*co*-hexafluoropropylene) blends and multilayer films

Jung-Kai Tseng, Kezhen Yin, Zhongbo Zhang, Matthew Mackey, Eric Baer, and Lei Zhu*

Department of Macromolecular Science and Engineering, Case Western Reserve University, Cleveland, Ohio 44106-7202, United States

* Corresponding author. E-mail address: lxz121@case.edu (L. Zhu).

I. X-ray Study of Nonstretched and Stretched PMMA/P(VDF-HFP) Blend Films

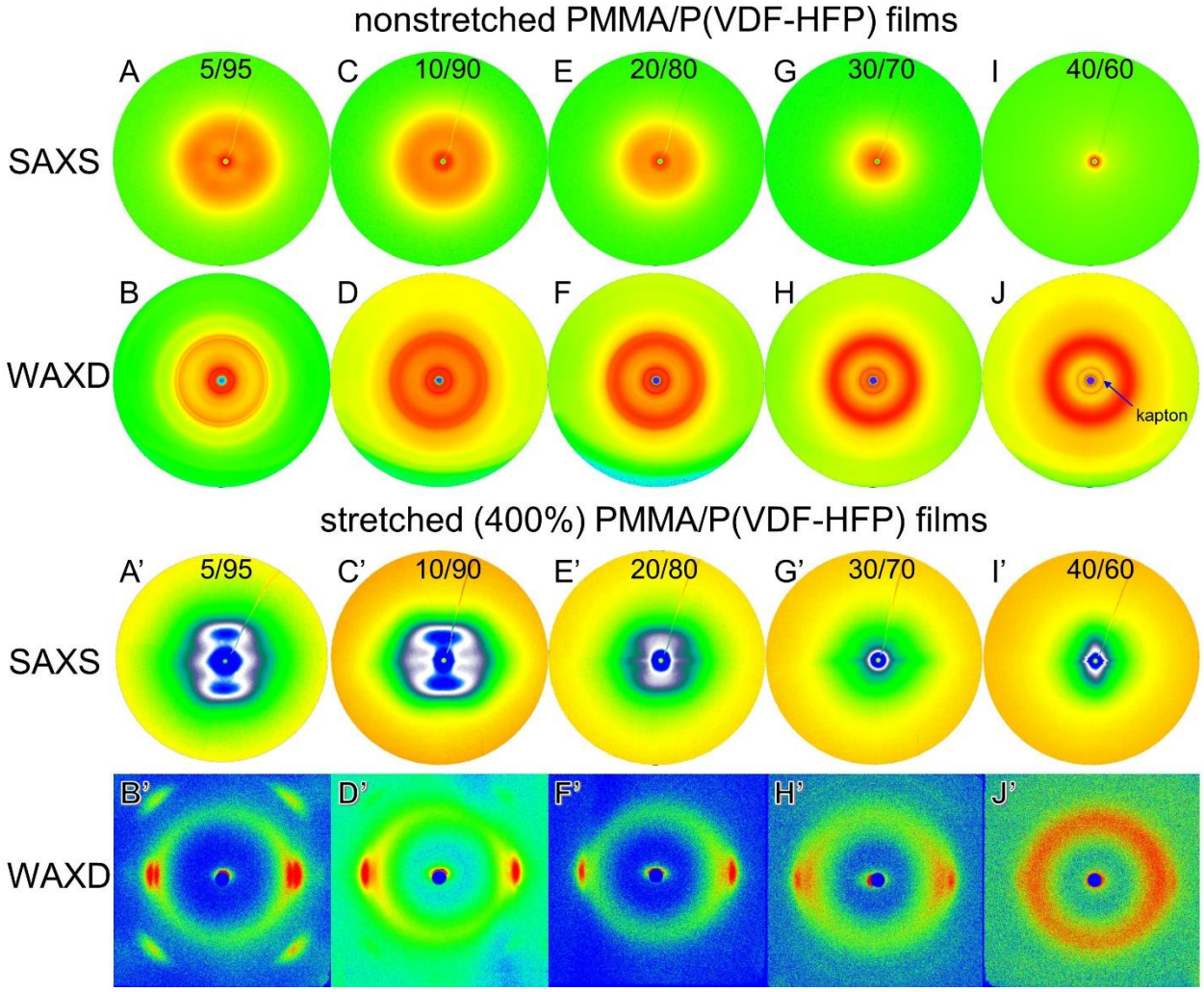

Figure S1. Two-dimensional (2D) SAXS and WAXD patterns for (the top panel) nonstretched and (the bottom panel) 400% stretched PMMA/P(VDF-HFP) blend films with different weight compositions of PMMA.

II. Effect of Draw Ratio on Crystalline Morphology and Ferroelectric Property of PMMA/P(VDF-HFP) Blend Films

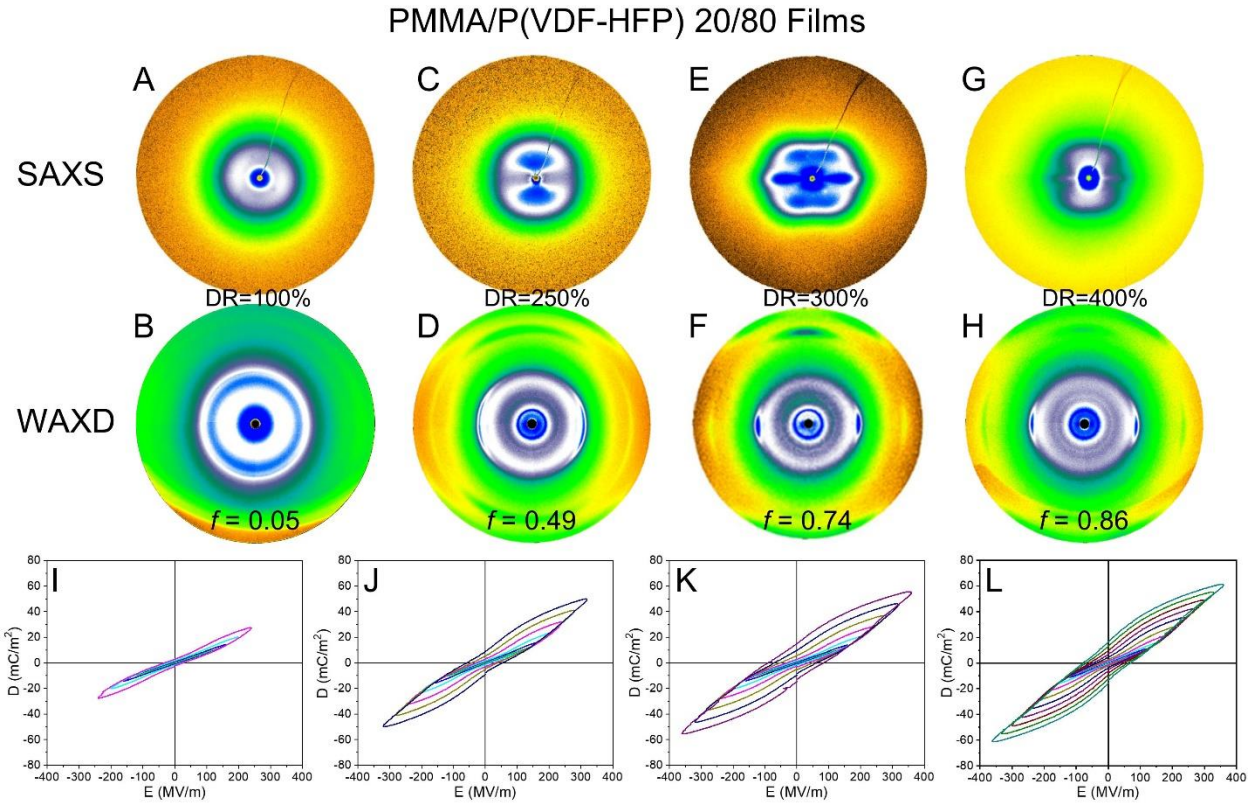

Figure S2. (Top panel) 2D SAXS and WAXD patterns for the stretched PMMA/P(VDF-HFP) 20/80 blend film with different draw ratios. The Herman orientation factor (*f*) values are shown in the WAXD patterns. (Bottom panel) Bipolar D-E loops for the stretched PMMA/P(VDF-HFP) 20/80 blend film with different draw ratios.

III. Bipolar D-E Loops for Various PMMA/P(VDF-HFP) Blend Films at 50 and 75 °C

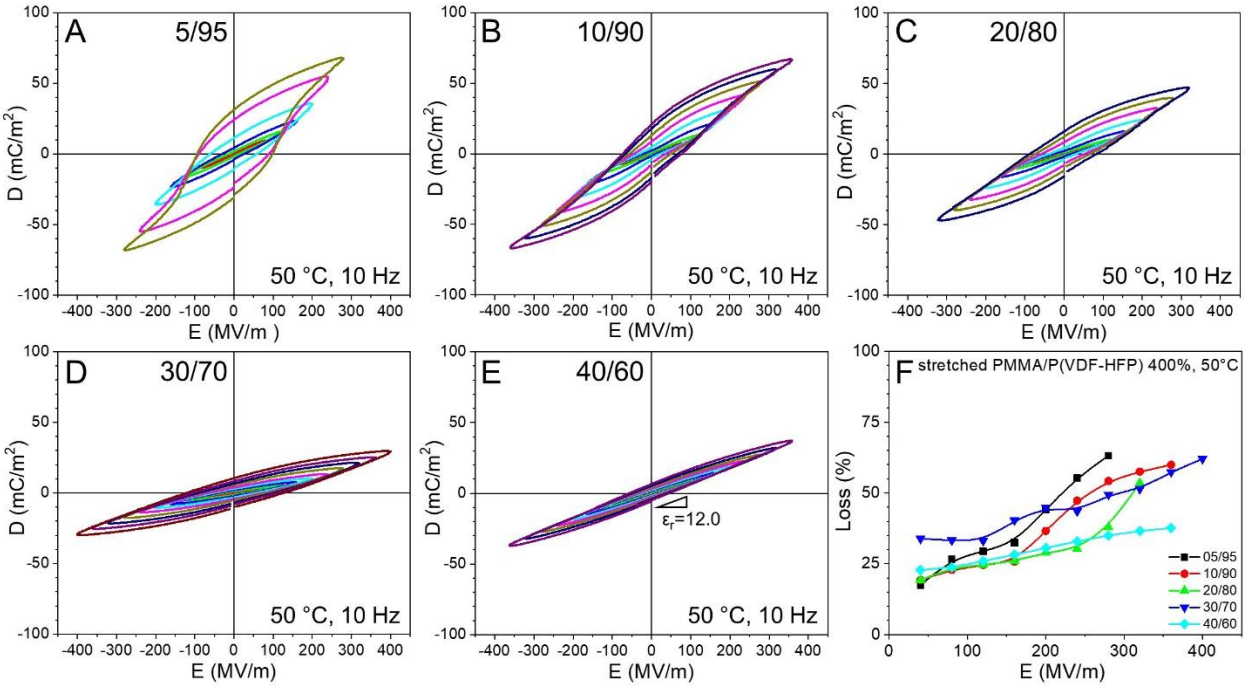

Figure S3. Bipolar D-E loops for PC/P(VDF-HFP) blend films: (A) 10/90, (B) 30/70, (C) 50/50, (D) 70/30, and (E) 90/10 (vol./vol.) at 50 °C. The poling frequency was 10 Hz with a sinusoidal wave function. (F) shows the loss% as a function of electric field for different blend films.

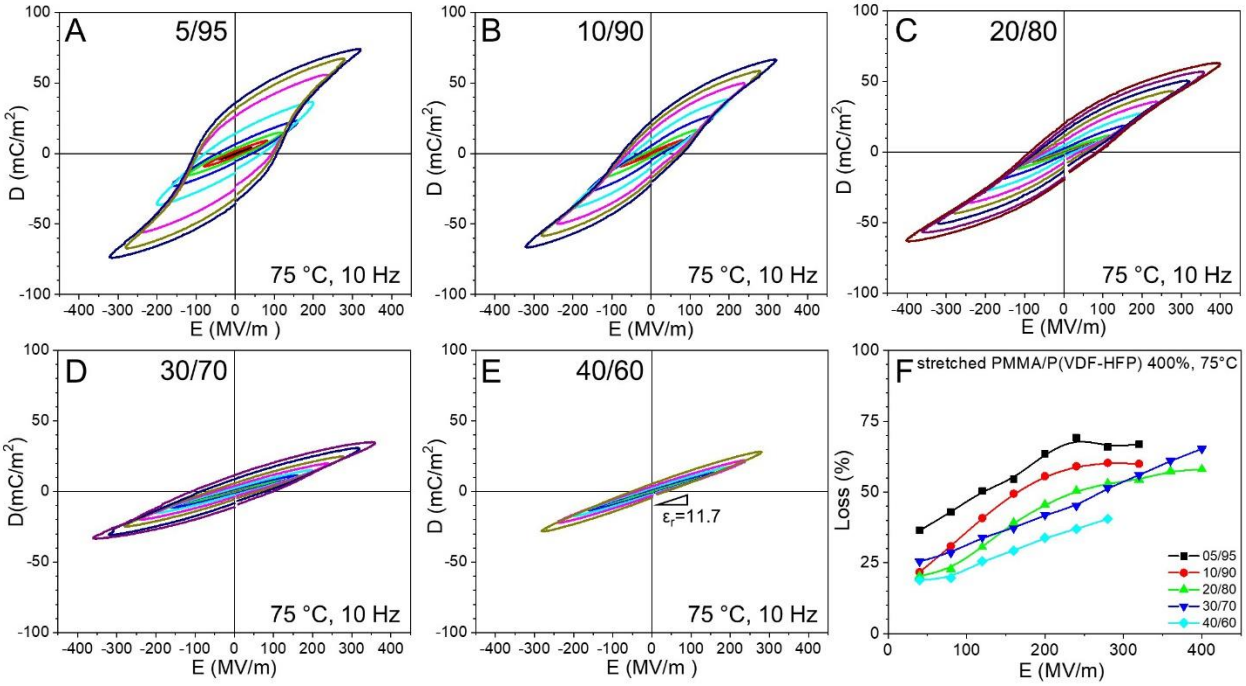

Fig. S4. Bipolar D-E loops for PC/P(VDF-HFP) blend films: (A) 10/90, (B) 30/70, (C) 50/50, (D) 70/30, and (E) 90/10 (vol./vol.) at 75 °C. The poling frequency was 10 Hz with a sinusoidal wave function. (F) shows the loss% as a function of electric field for different blend films.

IV. Frequency-scan BDS for Various PMMA/P(VDF-HFP) Blend Films at Various Temperatures

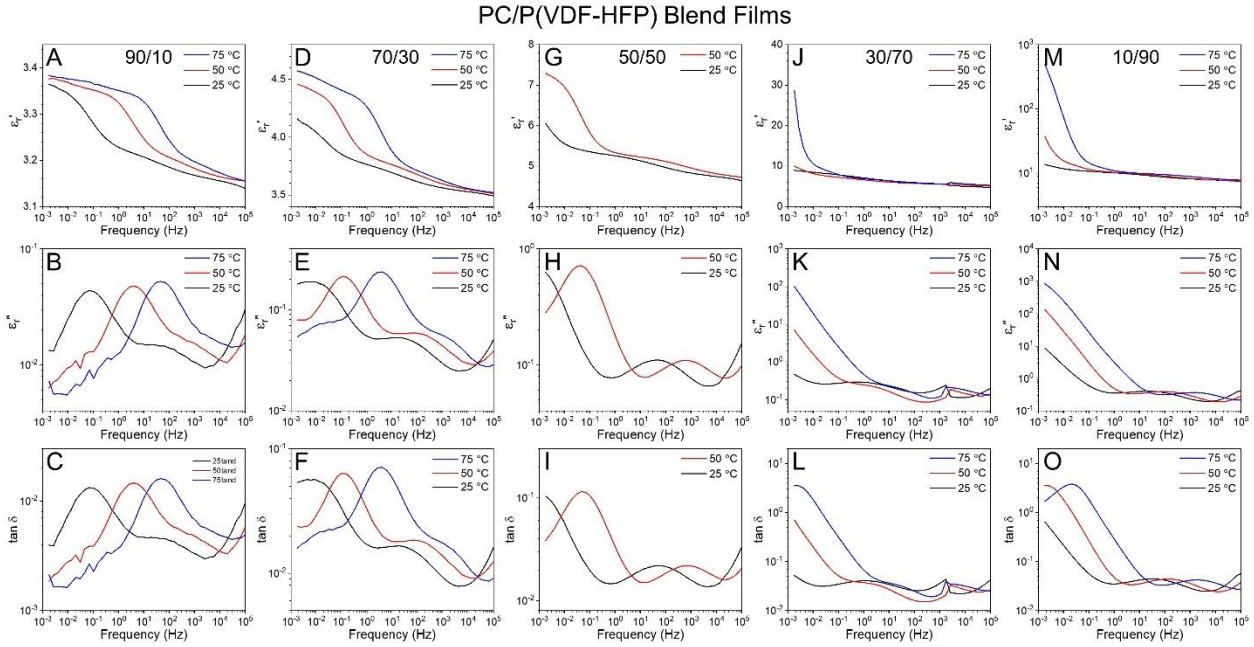

Fig. S5. Frequency-scan BDS results for PC/P(VDF-HFP) blend films, (A-C) 90/10, (D-F) 70/30, (G-I) 50/50, (J-L) 30/70, and (M-O) 10/90 at different temperatures: (A,D,G,J,M) ε_r', (B,E,H,K,N) ε_r'', and (C,F,I,L,O) dissipation factor, tanδ.

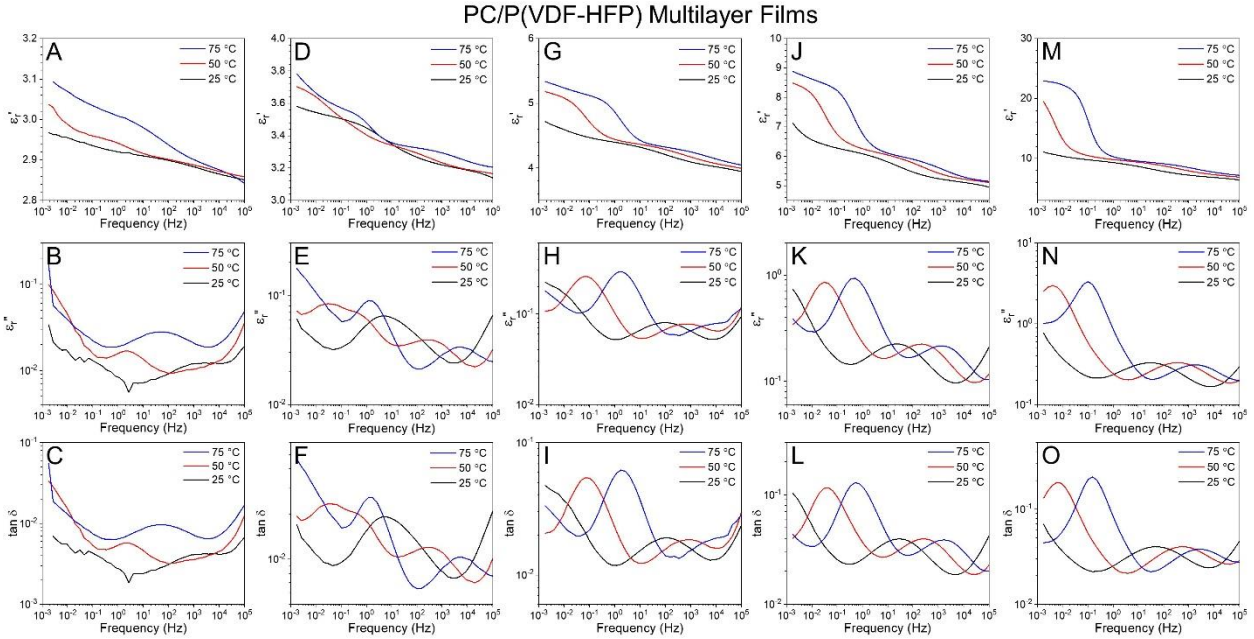

Fig. S6. Frequency-scan BDS results for PC/P(VDF-HFP) multilayer films, (A-C) 90/10, (D-F) 70/30, (G-I) 50/50, (J-L) 30/70, and (M-O) 10/90 at different temperatures: (A,D,G,J,M) ε_r', (B,E,H,K,N) ε_r'', and (C,F,I,L,O) dissipation factor, tanδ.

V. Derivation of ε_r', ε_r'', and tanδ for Parallel and Series Capacitor Models

For the parallel capacitor model, the overall capacitance (C_p^*) is:

$$C_p^* = C_1^* + C_2^* \quad \text{S1}$$

where C_1^*, C_2^* are complex capacitance of individual capacitors. Since capacitance is a function of area (A) and thickness (d) of the films, $C_i^* = \varepsilon_{r,i}^* \varepsilon_0 (A_i/d)$, where $\varepsilon_{r,i}^*$ is the complex permittivity and ε_0 is vacuum permittivity, we have:

$$\varepsilon_r^* \varepsilon_0 \frac{A}{d} = \varepsilon_{r1}^* \varepsilon_0 \frac{A_1}{d} + \varepsilon_{r2}^* \varepsilon_0 \frac{A_2}{d} \quad \text{S2}$$

$$\varepsilon_r^* = \varepsilon_{r1}^* \phi_1 + \varepsilon_{r2}^* \phi_2 \quad \text{S3}$$

where ε_r^* is the complex permittivity of the parallel capacitor model, ϕ_1 and ϕ_2 are volume fraction of capacitors 1 and 2. Since $\varepsilon_r^* = \varepsilon_r' - i\varepsilon_r''$ and $\tan\delta = \varepsilon_r''/\varepsilon_r'$, we can have:

$$\varepsilon_r' = \varepsilon_{r1}' \phi_1 + \varepsilon_{r2}' \phi_2 \quad \text{S4}$$

$$\varepsilon_r'' = \varepsilon_{r1}'' \phi_1 + \varepsilon_{r2}'' \phi_2 \quad \text{S5}$$

$$tan\delta = \frac{\varepsilon_{r1}'' \phi_1 + \varepsilon_{r2}'' \phi_2}{\varepsilon_{r1}' \phi_1 + \varepsilon_{r2}' \phi_2} \quad \text{S6}$$

For series capacitors, the overall capacitance C_s^*:

$$\frac{1}{C_s^*} = \frac{1}{C_1^*} + \frac{1}{C_2^*} \quad \text{S7}$$

Since $C_i^* = \varepsilon_{r,i}^* \varepsilon_0 (A/d_i)$, we have:

$$\frac{d}{\varepsilon_r^*} = \frac{d_1}{\varepsilon_{r1}^*} + \frac{d_2}{\varepsilon_{r2}^*} \quad \text{S8}$$

$$\frac{1}{\varepsilon_r^*} = \frac{\phi_1}{\varepsilon_{r1}^*} + \frac{\phi_2}{\varepsilon_{r2}^*} \quad \text{S9}$$

Since $\varepsilon_r^* = \varepsilon_r' - i\varepsilon_r''$ and $\tan\delta = \varepsilon_r''/\varepsilon_r'$, we can have:

$$\frac{\varepsilon_r'}{\varepsilon_r'^2 + \varepsilon_r''^2} = \frac{\phi_1 \varepsilon_{r1}'}{\varepsilon_{r1}'^2 + \varepsilon_{r1}''^2} + \frac{\phi_2 \varepsilon_{r2}'}{\varepsilon_{r2}'^2 + \varepsilon_{r2}''^2} \quad \text{S10}$$

$$\frac{\varepsilon_r''}{\varepsilon_r'^2 + \varepsilon_r''^2} = \frac{\phi_1 \varepsilon_{r1}''}{\varepsilon_{r1}'^2 + \varepsilon_{r1}''^2} + \frac{\phi_2 \varepsilon_{r2}''}{\varepsilon_{r2}'^2 + \varepsilon_{r2}''^2} \quad \text{S11}$$

$$\frac{tan\delta/\varepsilon_r'}{1+(tan\delta)^2} = \frac{\phi_1 tan\delta_1/\varepsilon_r'}{1+(tan\delta_1)^2} + \frac{\phi_2 tan\delta_2/\varepsilon_r'}{1+(tan\delta_2)^2} \quad \text{S12}$$

In the above derivation, any conduction is ignored. These theoretical predictions are shown in Fig. 6 in the main text.